Frontiers in Bioscience Landmark

Front. Biosci. (Landmark Ed) **2026**; 31(3): 47627
https://doi.org/10.31083/FBL47627

Original Research

Bioinformatics-Based Identification and Clinical Validation of CHST1 as a Potential Prognostic Gene Associated With EMT in Gastric Cancer

Xufu Qin[1,2,†], Yu Han[1,†], Zetao Wang[1,3], Xiaohui Zhou[1], Lijun Shi[1,*]

[1]Department of Gastroenterology, The First Affiliated Hospital of Harbin Medical University, 150001 Harbin, Heilongjiang, China
[2]Department of Gastroenterology, Heilongjiang Provincial Hospital, 150036 Harbin, Heilongjiang, China
[3]Fifth Department of Medicine (Nephrology/Endocrinology/Rheumatology, Pneumonology), University Medical Center Mannheim, University of Heidelberg, 68167 Mannheim, Baden-Wurttemberg, Germany
*Correspondence: 1433@hrbmu.edu.cn (Lijun Shi)
[†]These authors contributed equally.

Academic Editor: Amancio Carnero Moya
Submitted: 23 October 2025 Revised: 23 January 2026 Accepted: 3 February 2026 Published: 19 March 2026

Abstract

Background: Gastric cancer (GC) is among the most frequently diagnosed malignancies worldwide. Identifying novel therapeutic targets is of great significance. **Methods**: GC-related RNA-seq data and matched clinical information were retrieved from the publicly available The Cancer Genome Atlas (TCGA) database. The epithelial-mesenchymal transition (EMT) scores of GC and normal tissues were calculated using the gene set variation analysis (GSVA) package. Weighted gene coexpression network analysis (WGCNA) was applied to identify modules associated with EMT. The survival and clinical relevance of EMT-related core genes were analyzed, and carbohydrate sulfotransferase 1 (CHST1) was selected for further investigation. CHST1 expression was validated in patient-derived GC tissues and GC cell lines. Subsequently, CHST1 expression and mitogen-activated protein kinase (MAPK)/extracellular signal-regulated kinase (ERK) signaling pathway activity were modulated in AGS cells to evaluate their effects on cell proliferation, apoptosis, migration, and EMT. *In vivo* experiments were conducted to elucidate the involvement of CHST1 expression in GC growth. **Results**: The EMT score was markedly higher in GC tissues than in normal tissues. Within the EMT-related module, 7 hub genes (*CHST1*, *GPR176*, *OLFML2B*, *P4HA3*, *PDGFRB*, *SPARC*, and *VCAN*) were closely associated with GC prognosis. CHST1 expression was strongly correlated with both the EMT score and T stage. As revealed by survival analysis, patients with high CHST1 expression had shorter overall survival than those with low expression. A marked up-regulation of CHST1 protein expression was observed in clinical GC tissues compared with normal tissues. *In vitro*, CHST1 expression was significantly elevated in GC cell lines. Inhibiting CHST1 expression in AGS and HGC27 cells suppressed cell proliferation, migration, as well as EMT, while simultaneously promoting apoptosis. In AGS cells, CHST1 regulated cell proliferation, apoptosis, migration, and EMT through the MAPK/ERK signaling pathway. *In vivo*, CHST1 significantly promoted GC growth and increased the activity of the MAPK/ERK signaling pathway. **Conclusion**: CHST1 is highly expressed in GC and may influence GC progression by regulating the MAPK/ERK signaling pathway.

Keywords: CHST1; gastric cancer; epithelial-mesenchymal transition; prognosis

1. Introduction

Gastric cancer (GC) represents a critical public health concern globally, with an extremely high incidence and a correspondingly high mortality rate. Each year, over one million individuals are diagnosed with GC, making it ranks fifth in incidence and fourth in mortality among all cancers worldwide [1]. The incidence of GC exhibits marked geographic variation, with East Asia demonstrating the highest prevalence and Eastern and Central Europe ranking second [2]. Among countries worldwide, a high incidence of GC has been reported in China, posing a markedly serious threat to population health and survival [3]. Advanced age, *Helicobacter pylori* infection, high salt intake, as well as diets deficient in fruits and vegetables are recognized as major risk factors for GC. In recent years, a gradual reduction has been observed in both the frequency of new GC cases and the associated mortality [4]. Nevertheless, it is anticipated that the prevalence of GC would increase due to the aging of the global population. The overall prognosis of GC patients varies according to disease severity. For patients with early-stage GC, radical surgical resection remains the optimal treatment, achieving a 5-year survival rate of over 90% [5]. However, the absence of clear clinical manifestations in the initial phase of GC and patients' insufficient disease awareness result in nearly 70% of patients being diagnosed at a progressive or advanced stage. Approximately 30% of these patients have already lost the opportunity for radical surgical resection. Consequently, these patients face a dismal prognosis, with a median overall survival of only 3–4 months and an extremely low 5-year survival rate (only 3.17%) [6]. Unfortunately, current therapeutic options available for advanced GC are limited in their ability to substantially improve patient outcomes. As such, there is a pressing need to explore novel therapeutic approaches to address this unmet medical challenge.

Epithelial-mesenchymal transition (EMT) describes the process of epithelial cells' transdifferentiation into mesenchymal cells in response to certain physiological and pathological stimuli. EMT fulfills three major roles in the human body: (1) embryogenesis and organ development; (2) repair and healing of tissue injury; and (3) modulation of interactions between tumor cells, as well as between tumor cells and stroma, thereby promoting the invasion and metastasis of tumor cells [7]. Enhanced EMT has been reported to promote the invasion and progression of several types of tumors, including GC [8]. These findings demonstrate a strong correlation between EMT and progression of GC, offering key knowledge to facilitate the advancement of cutting-edge therapeutic approaches for the management of GC. The carbohydrate sulfotransferases (CHSTs) family comprises 15 members (CHST1–15), which are enzymes that catalyze the transfer of sulfate groups to glycosaminoglycans and other complex carbohydrates. CHSTs primarily reside in the cell membrane and cytoplasm, where they also function as structural components of the extracellular matrix (ECM) and facilitate tissue remodeling [9]. A study by Zhan *et al*. [9] reported that most CHSTs (CHST1, 2, 4, 5, 6, 11, 12, 13, 14, and 15) showed high expression in GC, suggesting their potential involvement in the progression of GC.

Tumors are pathological conditions that arise from genetic mutations, leading to uncontrolled cell proliferation. Advances in sequencing technologies and the advent of the genomic era have enabled molecular biologists to comprehensively analyze tumor genomes. Bioinformatics analysis of tumor genomes is capable of identifying new proto-oncogenes or oncogenes, thereby providing new methods for tumor diagnosis, clinical outcome prediction, and targeted therapy. Ultimately, these approaches offer valuable evidence to support the implementation of individualized tumor therapy [10]. In this study, a range of bioinformatics techniques were employed to determine key genes linked to the prognosis of GC. Critically, the link between CHST1 and GC progression was experimentally validated. Furthermore, we identified the regulatory role of CHST1 in the mitogen-activated protein kinase (MAPK)/extracellular signal-regulated kinase (ERK) signaling pathway. As is known, the MAPK signaling pathway is a widely conserved intracellular signal transduction mechanism. Its classical components include ERK1/2, JNK, p38 MAPK, and ERK5 [11]. Among these, ERK1 and ERK2 can recognize a variety of substrates, including transcription factors, protein kinases, and phosphatases [12]. Overactive MAPK signaling is observed in more than 85% of cancers, including HCC, GC [12–14]. Accumulating evidence suggests the involvement of the MAPK pathway in key cellular mechanisms of GC, including proliferation, invasion, migration, and metastasis, and that dysregulation of this signaling pathway contribute to the pathogenesis of GC [15]. Based on the aforementioned findings, the current study attempts to further clarify CHST1's role in GC and the potential underlying molecular mechanisms.

2. Materials and Methods

2.1 Data Retrieval and Processing

RNA-seq data and associated clinical data for GC were obtained from the publicly accessible The Cancer Genome Atlas-Stomach Adenocarcinoma (TCGA-STAD) project (https://portal.gdc.cancer.gov). This study included 448 samples in total, consisting of 36 control samples and 412 tumor samples. Only protein-coding genes were retained, and the expression of duplicates was averaged and normalization performed.

2.2 Screening for Differentially Expressed Genes (DEGs) in TCGA-STAD

The edgeR package in R (v 4.3.0, Walter and Eliza Hall Institute of Medical Research, Melbourne, VIC, Australia) was employed for conducting differential expression analysis on the TCGA-STAD samples, with $|\log FC| > 1$ & adjust. p value < 0.05. The EnhancedVolcano package (v 1.28.2, R package, St. Jude Children's Research Hospital, Memphis, TN, USA) was applied to generate volcano plots, and heatmaps displaying the top 20 up- and down-regulated genes were drawn with the pheatmap package (v1.0.13, R package, Raivo Kolde, Tartu, Estonia).

2.3 Functional Enrichment Analysis of DEGs

The clusterProfiler (v 4.18.4, R package, Guangchuang Yu, Southern Medical University, Guangzhou, Guangdong, China) and org.Hs.eg.db (v 3.22, R package, Marc Carlson, Fred Hutchinson Cancer Center, Seattle, WA, USA) packages were applied for performing Gene Ontology (GO) and Kyoto Encyclopedia of Genes and Genomes (KEGG) enrichment analyses, with the significance threshold set at $p < 0.05$. The corresponding analysis results were represented through bubble plots.

2.4 Evaluation of EMT Scores

EMT score calculation was performed using the GSVA package (v 3.22, R package, Robert Castelo, Universitat Pompeu Fabra, Barcelona, Catalonia, Spain) employing the HALLMARK_EPITHELIAL_MESENCHYMAL_TRANSITION gene set from the Molecular Signatures Database.

2.5 Identification of EMT-Related Modules

DEGs were subjected to weighted gene co-expression network analysis (WGCNA) via the WGCNA package (v 1.72-5, R package, Peter Langfelder and Steve Horvath, University of California, Los Angeles, CA, USA). Samples were clustered and analyzed for independence and average connectivity. Subsequently, a weighted co-expression network was constructed, and the green module (cor = 0.8, $p <$

0.01) that showed the highest relevance to the EMT score was selected as the key module.

2.6 Screening and Functional Enrichment Analysis of EMT-Related Genes

Key module genes were identified using criteria of Gene Significance (GS) >0.6 & Module Membership (MM) >0.6. Functional enrichment analysis of these genes was subsequently conducted, followed by visualization of GO and KEGG enrichment results using bubble maps.

2.7 Analysis of EMT-Related Prognostic Genes

The identified key module genes were subjected to survival analysis via the survival package (v 3.7, R package, Terry M. Therneau, Mayo Clinic, Rochester, MN, USA) in R. Kaplan–Meier curves were plotted with the ggsurvplot function. Genes showing significant association with survival time and rate were screened using the log-rank test, with a p value threshold of 0.01.

2.8 Correlation Analysis of CHST1 Expression and EMT Score

Analysis of gene expression was carried out based on the TCGA-STAD dataset. CHST1 expression-EMT score correlation was analyzed using the ggpubr package (v 0.6.0, R package, Alboukadel Kassambara, University of Debrecen, Debrecen, Hungary). Scatter plots were generated with the ggscatter function, incorporating a regression line, the Pearson correlation coefficient, along with its corresponding p-value. The sign and magnitude of the coefficient represent the direction and strength of the correlation between CHST1 expression and EMT, respectively.

2.9 Clinical Correlation Analysis of CHST1

Wilcoxon rank sum test was employed to analyze the correlation between the *CHST1* gene and relevant clinical characteristics in TCGA-STAD using the ggpubr package. In addition, based on the GSE84437 dataset from the Gene Expression Omnibus database, the correlation between CHST1 expression and clinical characteristics was further assessed, and survival analysis was conducted to examine the link between CHST1 expression and the overall survival in GC patients.

2.10 Validation of CHST1 Expression in GC Clinical Tissues

CHST1 expression was validated in tumor tissue samples obtained from patients with GC. The GC tissue samples were provided by the Department of Gastroenterology, The First Affiliated Hospital of Harbin Medical University. Ethical approval for the current study was granted by the Ethics Committee of The First Affiliated Hospital of Harbin Medical University (Approval No.: 2024314). All study participants voluntarily provided informed consent.

2.11 Immunohistochemistry (IHC)

Tumor sections embedded in paraffin underwent deparaffinization and rehydration, followed by antigen retrieval via microwave heating. Subsequently, the activity of endogenous peroxidase was blocked with hydrogen peroxide, and non-specific binding was reduced by incubation with normal goat serum. Subsequently, the sections were incubated sequentially with a primary anti-CHST1 antibody (1/200, 44627) overnight at 4 °C and a corresponding HRP-conjugated secondary antibody (Rabbit, 8114) at room temperature. Visualization was performed using DAB (P0202, Beyotime, China), with the reaction monitored under a microscope until distinct brownish-yellow granular staining was observed. Finally, the nuclei were counterstained with hematoxylin (C0107-100 mL, Beyotime, China). After dehydration and clearing, the sections were mounted with neutral resin and examined under a microscope (MoticAE 2000, MOTIC, China). Both antibodies for this experiment were acquired from Cell Signaling Technology, Inc. (CST, Danvers, MA, USA).

2.12 Establishment of Subcutaneous Graft Tumor Model

Approval for establishing the subcutaneous graft tumor model was granted by the Experimental Animal Welfare Ethics Committee of the First Affiliated Hospital of Harbin Medical University (IACUC NO. 2023068). 4–5-week-old male BALB/c nude mice (16–18 g) used in this experiment were supplied by Beijing Vital River Laboratory Animal Technology Co. Ltd. (China). These experimental mice were kept in pairs under standardized housing conditions and provided with autoclaved food and sterile water. The animal facility maintained controlled environmental parameters: temperature of 22 $\pm$ 2 °C, relative humidity of 55 $\pm$ 5%, and a 12-hour light/dark cycle. Following a five-day acclimation period, all mice were randomly assigned to three groups (AGS, AGS+shRNA, and AGS+sh-CHST1), each containing six mice. Specifically, mice were stratified by body weight and then distributed randomly into three groups (1:1:1) using block randomization generated by R software (v 4.22, R Foundation for Statistical Computing, Vienna, Austria) (set.seed = 123). The allocation scheme was concealed in sealed envelopes maintained by a technician not involved in the experiments, and investigators were blinded to group assignments during all experimental procedures and outcome assessment. AGS cells, shRNA-transfected AGS cells, and CHST1-shRNA (sh-CHST1)-transfected AGS cells were digested, resuspended with PBS, and injected into the left axillary region of nude mice according to group assignment, with 5×10^6 cells per injection. During the experimental period, mice had unrestricted access to both food and drinking water. Every four days, the tumors at the anterior axillary region were measured for length and width using calipers, and their volume was calculated using the following-listed formula: $V = \text{length} \times \text{width}^2/2$. After 14 days, mice were

anesthetized via intraperitoneal administration of Zoletil 50 (tiletamine-zolazepam, 50 mg/kg, 10 mg/mL) and subsequently humanely euthanized by the method of cervical dislocation. Next, tumor tissues were collected, photographed, measured, and weighed. The volume of the tumor was calculated, ensuring that no tumor exceeded 1500 mm^3 as permitted by the Institutional Animal Care and Use Committee. Tumor weights were recorded, and no deaths occurred throughout the entire experiment. The sequence of treatments and measurements was determined by cage position.

2.13 Cell Culture

Human GC cell lines (MKN28, HGC27, and AGS) and the human gastric mucosal epithelial cell line GES-1 were supplied by Wuhan Procell Life Sciences Co., Ltd. (China). All these cell lines underwent STR profiling for authentication and were tested negative for mycoplasma. They were cultured in DMEM (C11995500BT, Thermo Fisher Scientific, Waltham, MA, USA) containing 10% fetal bovine serum (NFBS-2500A, Noverse, USA), 100 U/mL penicillin (ST488-1, Beyotime, China), and 100 µg/mL streptomycin (ST488-2, Beyotime, China), and maintained at 37 °C in an incubator with 5% CO_2.

2.14 Cell Counting Kit-8 (CCK-8) Assay

96-well plates were seeded with logarithmically growing HGC27 cells (5000 cells/well) and AGS cells (3000 cells/per well) in 100 µL of culture medium. After 24, 48, or 72 h of incubation, 10 µL of CCK-8 solution (CK04, Solarbio, China) was added to each well, and the plates were further incubated at 37 °C for 2 h. MK-3 Microplate Reader (Thermo Fisher Scientific, USA) was employed to detect absorbance at 450 nm.

2.15 Cell Transfection and Treatment

Lentivirus expressing sh-CHST1 or shRNA (negative control), along with CHST1 overexpression plasmid (OE-CHST1) or the corresponding empty plasmid (OE-NC), was obtained from OBiO Technology (Shanghai) Corp., Ltd. (China). Lentivirus transfection was performed to achieve CHST1 knockdown in AGS and HGC27 cells. Accordingly, AGS and HGC27 cells were categorized into two groups: a negative control group (AGS+shRNA and HGC27+shRNA); and a CHST1 intervention group (AGS+sh-CHST1, HGC27+sh-CHST1). CHST1 was overexpressed in AGS cells using Lipofectamine™ 3000 transfection reagent (L3000015, Thermo Fisher Scientific, USA) with OE-CHST1. AGS cells were subsequently allocated into the following experimental groups: Control, SB203580, and SB203580+OE-CHST1. Both AGS cells and CHST1-overexpressing AGS cells were treated with 20 µmol/L SB203580 (a p38 MAPK inhibitor, HY-10256, MedChemExpress, USA).

Table 1. Primary antibodies.

Antibody	Dilution	Catalog number	Brand
GAPDH	1:1000	2118	CST
CHST1	1:800	44627	CST
E-cadherin	1:800	3195	CST
N-cadherin	1:800	13116	CST
vimentin	1:800	5741	CST
snail	1:800	3879	CST
p38 MAPK	1:1000	2410	CST
Phospho (p)-p38 MAPK	1:1000	4511	CST
ERK	1:1000	4695	CST
p-ERK	1:1000	9101	CST

2.16 Western Blot (WB)

The extracted total proteins from tissue or cell lysates in each group were quantified using a BCA assay kit (P0011, Beyotime, China). The collected protein samples were separated by electrophoresis using SDS-PAGE gels (12%) (P1200-25T, Solarbio, China) and next transferred onto polyvinylidene fluoride membranes (ISEQ00010, Millipore, Burlington, MA, USA). After being blocked in 5% skim milk, the membranes were subjected to an overnight incubation with primary antibodies (Table 1) at 4 °C, and subsequently with 1 h of incubation with the corresponding secondary antibody at room temperature. Target proteins were then detected using the chemiluminescent detection substrate (WBULS0500, Millipore, USA).

2.17 Immunofluorescence (IF)

GC cells of each strain (MKN28, HGC27, and AGS) and human gastric mucosal epithelial cells (GES-1) were inoculated onto anti-degradation slides. Cells were treated with 4% paraformaldehyde (BL539A, Biosharp, Hefei, Anhui, China) for fixation, followed by permeabilization with Triton X-100 (BS084-100 mL, Biosharp, China). After being blocked with 10% goat serum, the cells underwent an overnight incubation with primary antibodies against CHST1 (1:200, CST, USA), E-cadherin (1:200, CST, USA), vimentin (1:100, CST, USA), N-cadherin (1:400, CST, USA), and snail (1:200, CST, USA) at 4 °C, and then 1 h of incubation with fluorescently coupled secondary antibodies (4412, 1:1000, Alexa Fluor® 488, CST, USA) at room temperature. Subsequently, the cell nuclei were stained with DAPI (D9542, Millipore, USA) and photographed using a fluorescence microscope (Axio Observer. A1, Zeiss, Germany).

2.18 RNA Extraction and qRT-PCR Analysis

RNA of the control and CHST1-intervention groups were extracted using Trizol solution (15596026, Thermo Fisher Scientific, USA) and then reverse-transcribed into cDNA (RR037Q, Takara, China). qPCR (CN830S, Takara, China) was performed, with PCR reaction conditions as follows: 95 °C for 10 min, followed by 40 cycles of 95

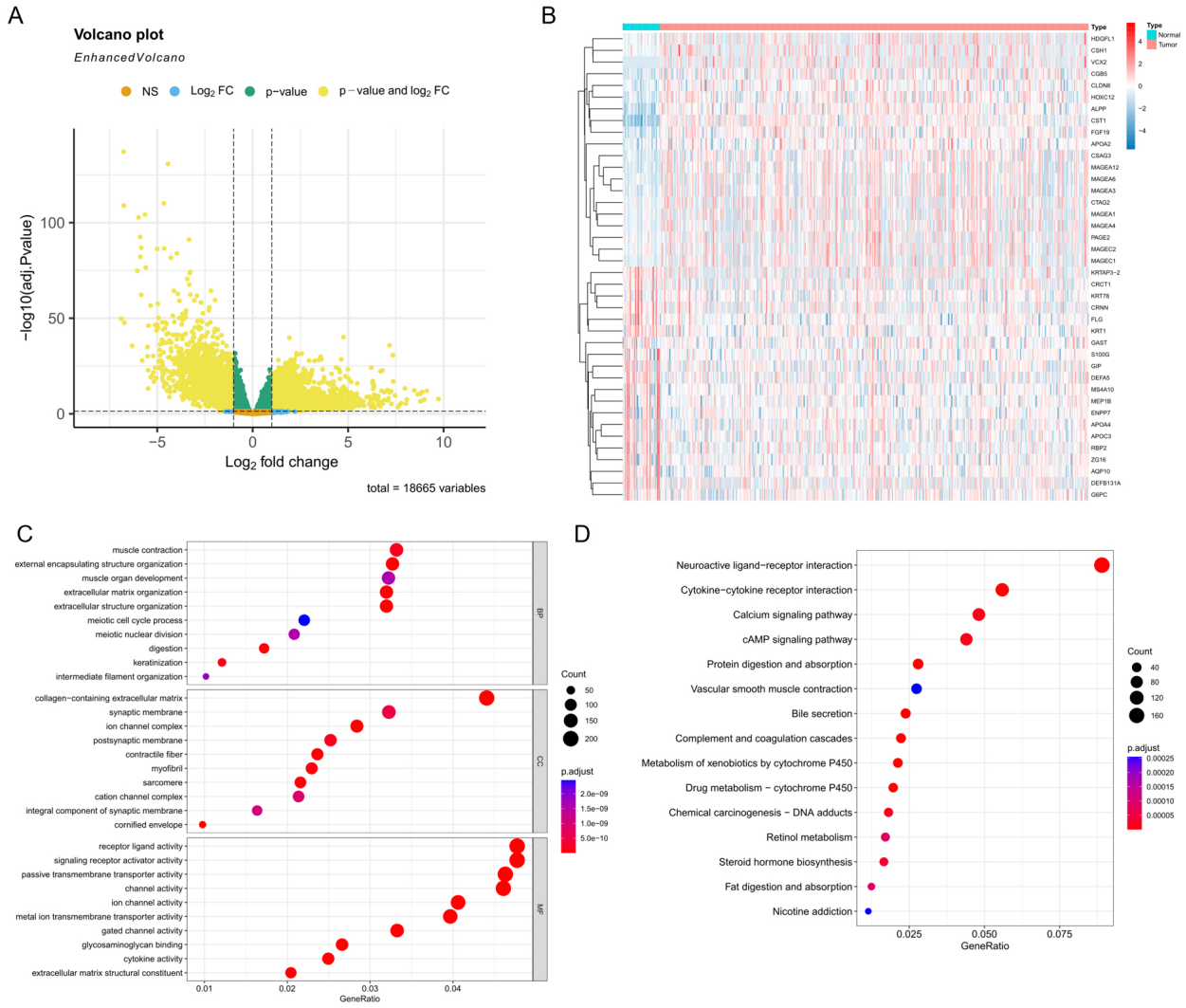

Fig. 1. Screening and enrichment analysis of DEGs in GC. (A) Volcano plot of DEGs. (B) Heatmap of the top 20 up- and down-regulated DEGs. (C) GO enrichment analysis of DEGs. (D) KEGG pathway enrichment analysis of DEGs. DEGs, Differentially Expressed Genes; GC, gastric cancer; GO, Gene Ontology; KEGG, Kyoto Encyclopedia of Genes and Genomes.

°C for 30 s, 60 °C for 30 s, and 72 °C for 1 min. The $2^{-\Delta\Delta Ct}$ method was applied for calculating the relative level of CHST1 expression. The primer sequences were as follows: CHST1-F: GGTGGGTCTGGGTCTAGGAT; CHST1-R: GGGAGGAAGCACAGCAGATT; β-actin-F: CAGATGTGGATCAGCAAGCAGGAG; and β-actin-R: CGCAACTAAGTCATAGTCCGCCTAG.

2.19 Plate Cloning Assay

During the logarithmic growth phase, AGS and HGC27 cells were inoculated in 6-well plates (1×10^3 cells/well). After two weeks of culture, the cell cloning in each well was observed. The cells were then washed with PBS (three times, 5 min/time), pre-cooled with methanol fixation at 4 °C for 20 min, stained with crystal violet for 1 h, rinsed with ultrapure water, dried, and photographed with an inverted microscope.

2.20 Cell Scratching Assay

Cells were seeded into 6-well plates and grown to approximately 90% confluence. A scratch perpendicular to the labeled line was created using a 100 µL sterile pipette. Images of the scratch were captured at the same observation point. The width of the scratch was measured at 0 and 24 h, followed by calculation of the wound healing rate.

2.21 Flow Cytometry Analysis

Flow cytometry (FACS Calibur, BD, USA) was used to quantify apoptosis. After resuspension in 300 µL of binding buffer, cells were treated with Annexin V-FITC (5 µL) and incubated for 10 min. Subsequently, propidium iodide (5 µL) staining was performed for 5 min in the dark, and FlowJo V10 software (BD Biosciences, Ashland, OR, USA) was applied to analyze apoptosis.

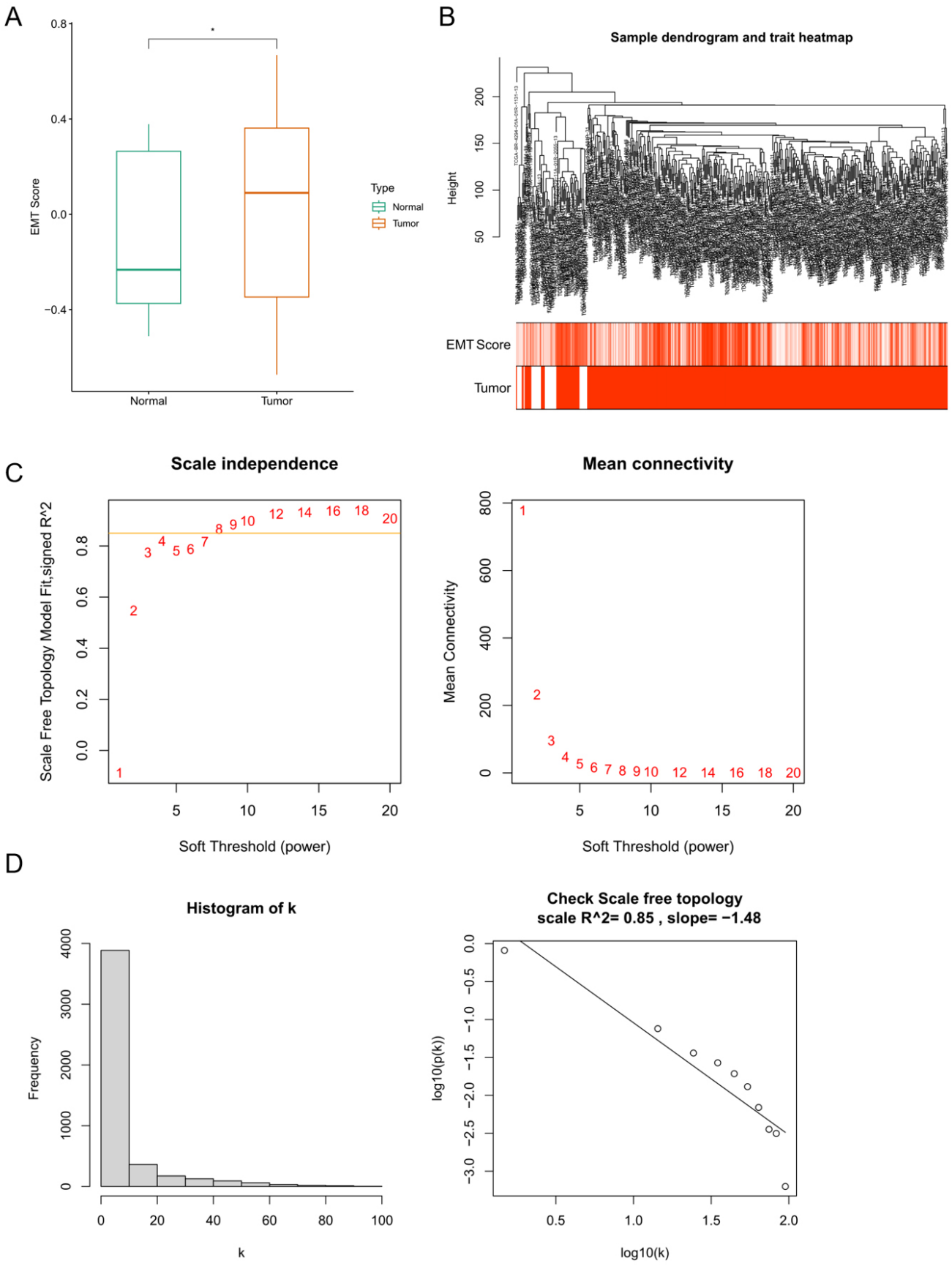

Fig. 2. EMT score and WGCNA. (A) Comparison of EMT scores between tumor and normal tissues. (B–D) WGCNA of DEGs in GC. * $p < 0.05$. EMT, epithelial-mesenchymal transition; WGCNA, weighted gene co-expression network analysis.

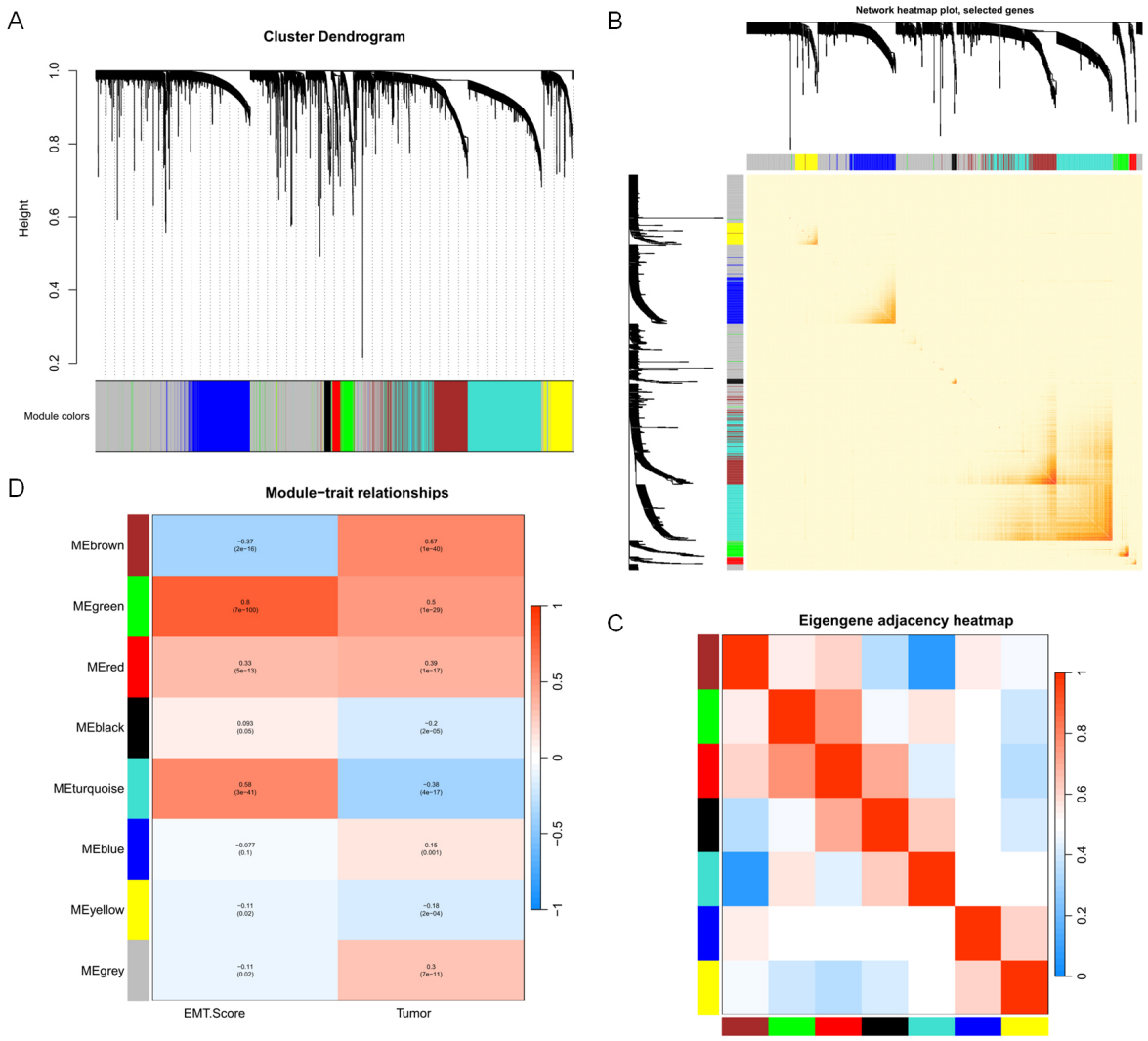

Fig. 3. Screening of EMT-related modules. (A–C) Weighted gene co-expression network and heatmap of correlation between modules. (D) Correlation analysis of each module with EMT score and tumor.

2.22 Statistical Analysis

R software was employed for performing bioinformatics analysis. No pre-established exclusion criteria were defined for animals or data points in this experiment. All analyses were performed using the original complete dataset. For statistical purposes, each group included three independent cell data or the data of six mice. During the experimental procedures, the first author was aware of the group allocations. The data were subjected to statistical analysis using SPSS 22.0 (IBM Corp., Armonk, NY, USA). The data were reported as mean $\pm$ standard deviation (SD). All statistical data were evaluated for normality and homogeneity of variance. The Student's *t*-test was applied for pairwise comparisons, while comparisons among three or more groups were carried out using one-way ANOVA followed by Sidak's multiple comparisons test. $p < 0.05$ denotes a statistically significant difference.

3. Results

3.1 Screening of DEGs and Enrichment Analysis for TCGA-STAD

Comparative analysis between tumor and normal samples revealed 4765 DEGs in total. Among these DEGs, there were 2542 up-regulated and 2223 down-regulated genes (Fig. 1A). Heatmap showing the top 20 up- and down-regulated genes is presented in Fig. 1B. Functional enrichment analyses were subsequently conducted on these identified DEGs. GO enrichment analysis revealed that, the DEGs were mainly enriched in ECM and extracellular structure organization (BP category); collagen-containing ECM (CC category); and receptor ligand activity and signaling receptor activator activity (MF category) (Fig. 1C). KEGG pathway analysis indicated enrichment of these DEGs in the neuroactive ligand-receptor interaction (Fig. 1D).

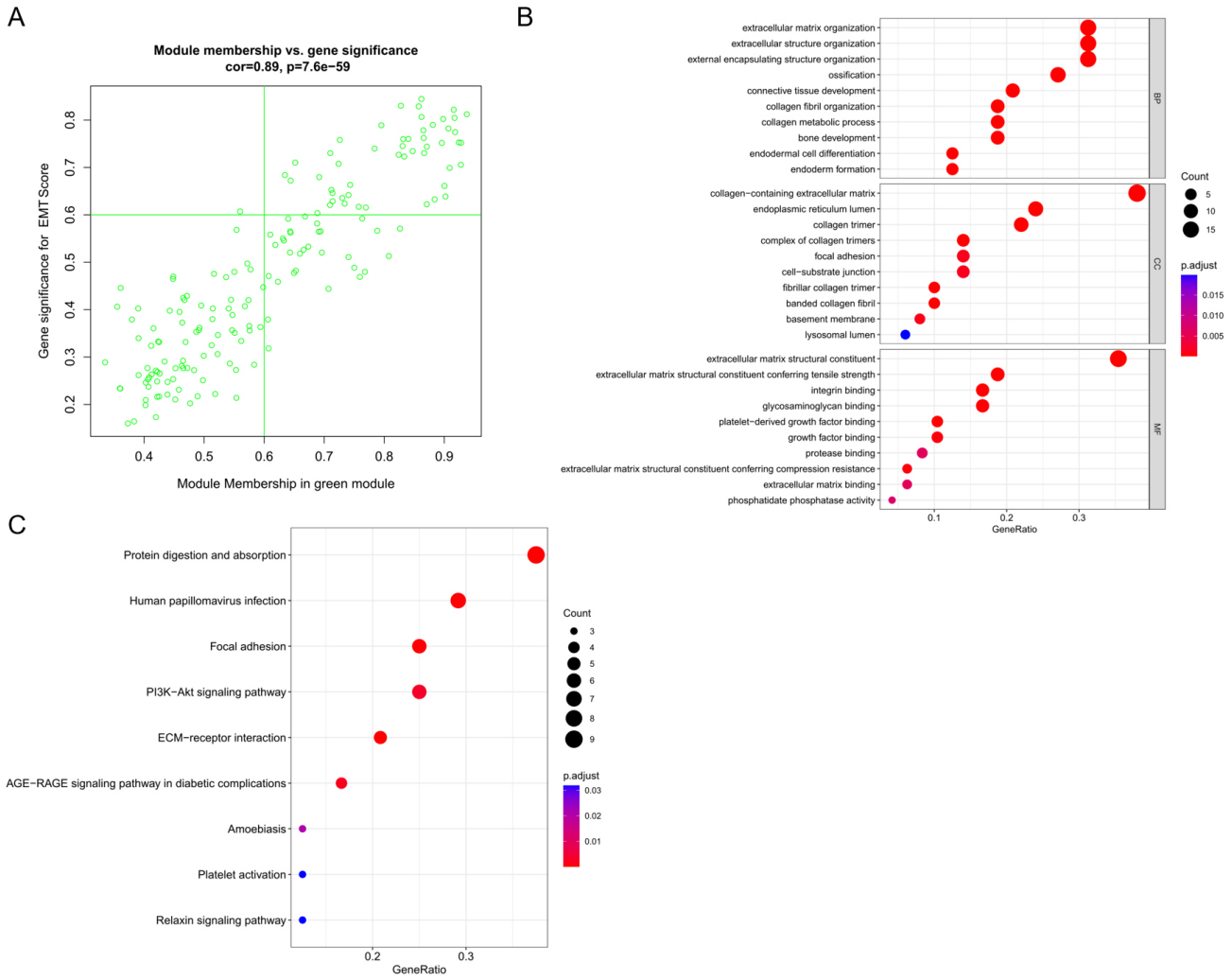

Fig. 4. Screening of EMT-related genes and functional enrichment analysis. (A) Screening of EMT-related genes. (B) GO enrichment analysis of EMT-related genes. (C) KEGG pathway enrichment analysis of EMT-related genes.

3.2 EMT Score and WGCNA

The EMT score was calculated for all samples, revealing a marked elevation in tumor group relative to normal group ($p < 0.05$) (Fig. 2A). WGCNA was subsequently performed on the 4,765 DEGs to generate a heat map of sample clustering and clinical features (Fig. 2B). A power value of 8 was selected (Fig. 2C), corresponding to a R^2 of 0.85 and a slope of –1.48 (Fig. 2D).

3.3 Screening of EMT-Related Modules

A weighted gene co-expression network (Fig. 3A) was constructed, and the transcriptome overview map plots (Fig. 3B) and correlation heatmaps between modules (Fig. 3C) were generated. Subsequently, correlation analysis between sample characteristics (EMT score, tumor) and the modules was performed (Fig. 3D). The results showed that, among all modules, the green module (cor = 0.8, $p <$ 0.01) exhibited the strongest correlation and was thus defined as the key module, comprising 169 genes.

3.4 Screening of EMT-Related Genes and Functional Enrichment Analysis

GS *vs.* MM analysis (Fig. 4A) was performed on the key module, and 50 key module genes were obtained by filtering with thresholds of GS >0.6 & MM >0.6. Functional enrichment analysis was subsequently conducted on the key module genes. GO enrichment analysis revealed that the key module genes were primarily enriched in extracellular structure organization, ECM organization, and external encapsulating structure organization (BP category); collagen-containing ECM (CC category); and ECM structural constituent (MF category) (Fig. 4B). KEGG pathway analysis indicated significant enrichment in protein digestion and absorption (Fig. 4C).

3.5 Prognostic Analysis of EMT-Related Genes

Survival analysis of the 50 EMT-related genes (Fig. 5) revealed seven genes significantly associated with survival: *CHST1*, *GPR176*, *OLFML2B*, *P4HA3*, *PDGFRB*, *SPARC*,

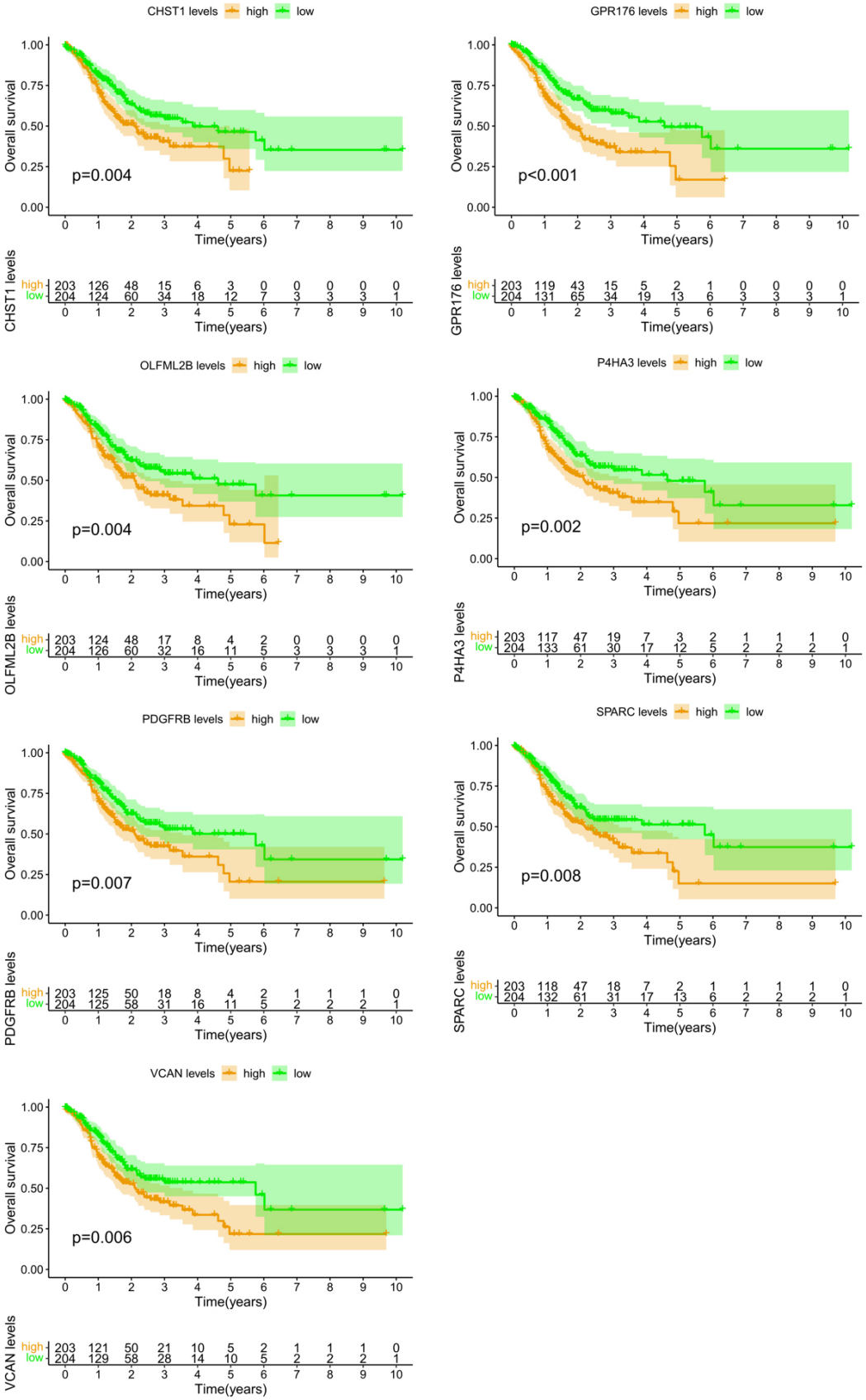

Fig. 5. Prognostic analysis of EMT-related genes. CHST1, carbohydrate sulfotransferase 1; GPR176, G protein-coupled receptor 176; OLFML2B, olfactomedin-like 2B; P4HA3, prolyl 4-hydroxylase subunit alpha 3; PDGFRB, platelet-derived growth factor receptor beta; SPARC, secreted protein acidic and cysteine rich; VCAN, versican.

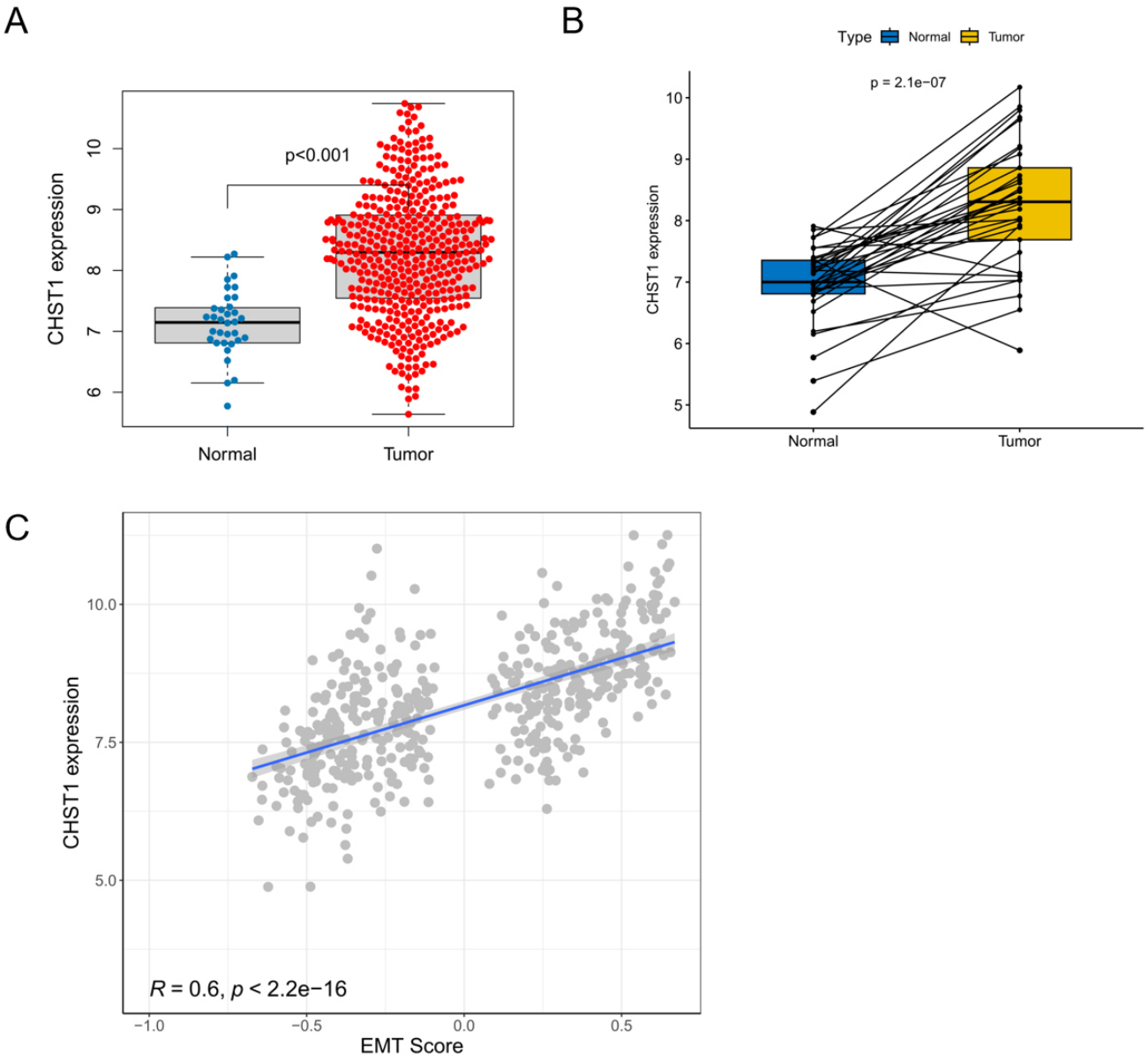

Fig. 6. Correlation analysis between CHST1 and EMT score. (A,B) Comparison of CHST1 expression between the tumor and normal groups. (C) Correlation analysis of CHST1 expression with EMT Score. CHST1, carbohydrate sulfotransferase 1; EMT, epithelial-mesenchymal transition.

and *VCAN*, which were defined as hub genes. Among these, *CHST1* demonstrates high expression in GC tissues; nevertheless, the underlying mechanism remains unclear. As such, *CHST1* was selected for subsequent analysis in this study.

3.6 Correlation Analysis of CHST1 and EMT Score

Significant expression of CHST1 was found in the tumor group in comparison to the normal group ($p < 0.001$) (Fig. 6A,B). Furthermore, a notable and statistically significant positive correlation was observed between CHST1 expression and the EMT score (R = 0.6, $p < 0.001$) (Fig. 6C).

3.7 Clinical Correlation Analysis of CHST1

Clinical correlation analysis demonstrated a significant correlation between CHST1 expression and T-stage ($p < 0.001$), whereas no marked correlation was observed between CHST1 expression and other clinical features, including gender, age, tumor grade, M-stage, N-stage, or stage ($p > 0.05$) (Fig. 7).

Subsequently, the GSE84437 dataset (comprising 433 GC samples) was analyzed to evaluate the association between CHST1 expression and clinical characteristics/patient survival. It was revealed through analysis of clinical features that CHST1 expression was markedly associated with T-stage but not with age, gender, or N-stage

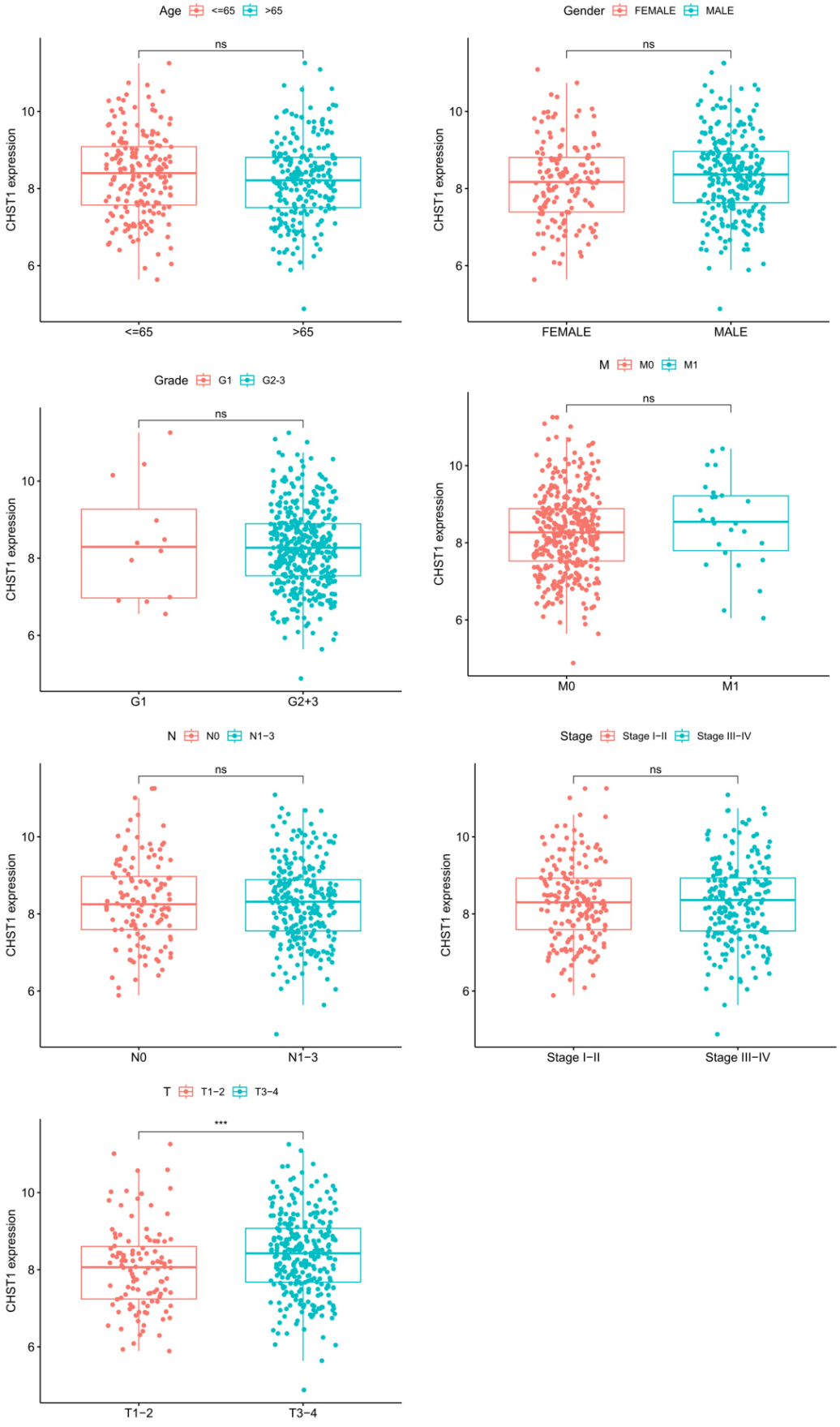

Fig. 7. Clinical correlation analysis of CHST1. ns: $p > 0.05$, *** $p < 0.001$.

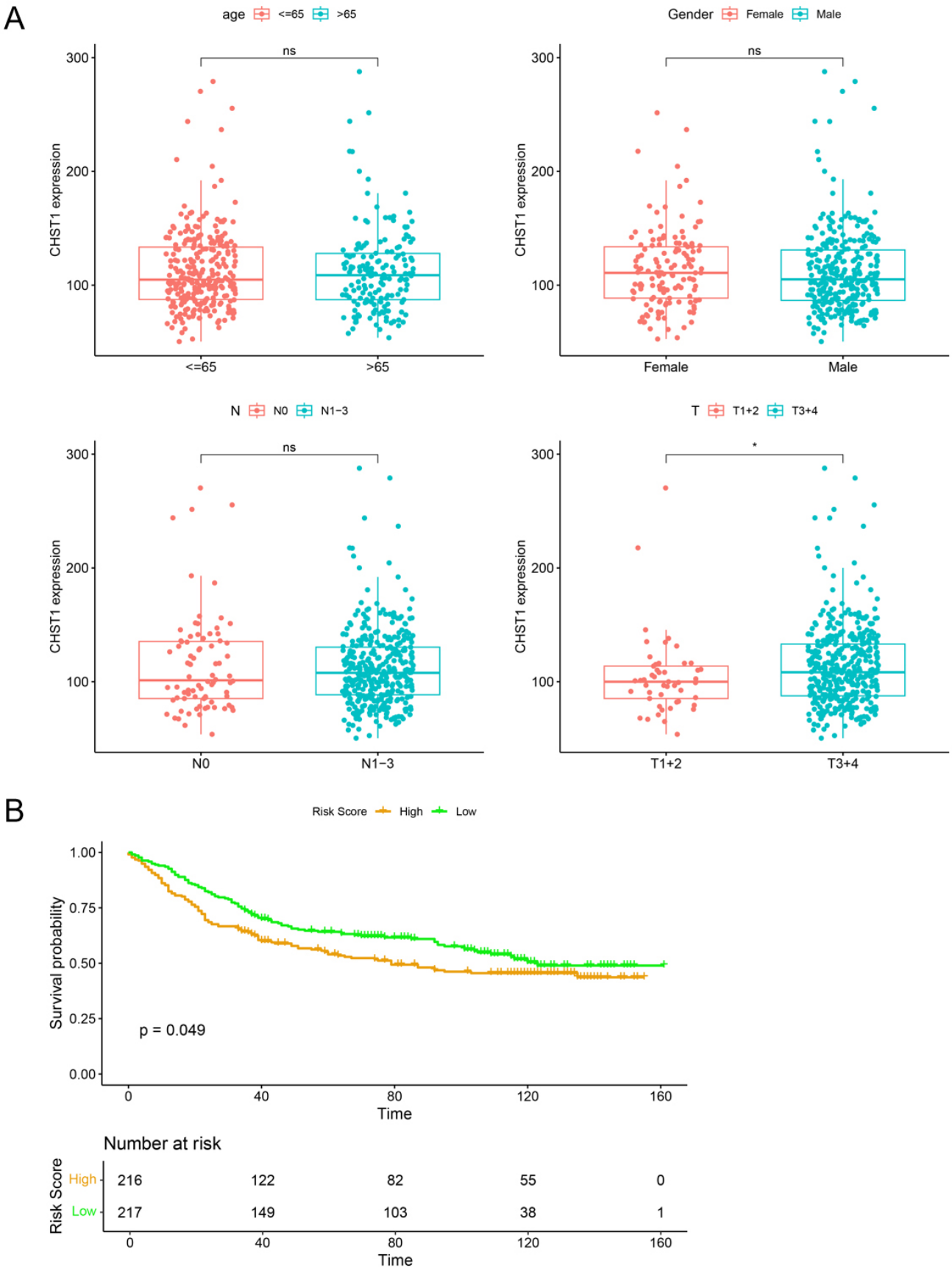

Fig. 8. Clinical correlation analysis and survival analysis of CHST1. (A) Correlation analysis of CHST1 expression with age, gender, N-stage, and T-stage in GC patients. (B) Survival analysis of CHST1. ns: $p > 0.05$, * $p < 0.05$.

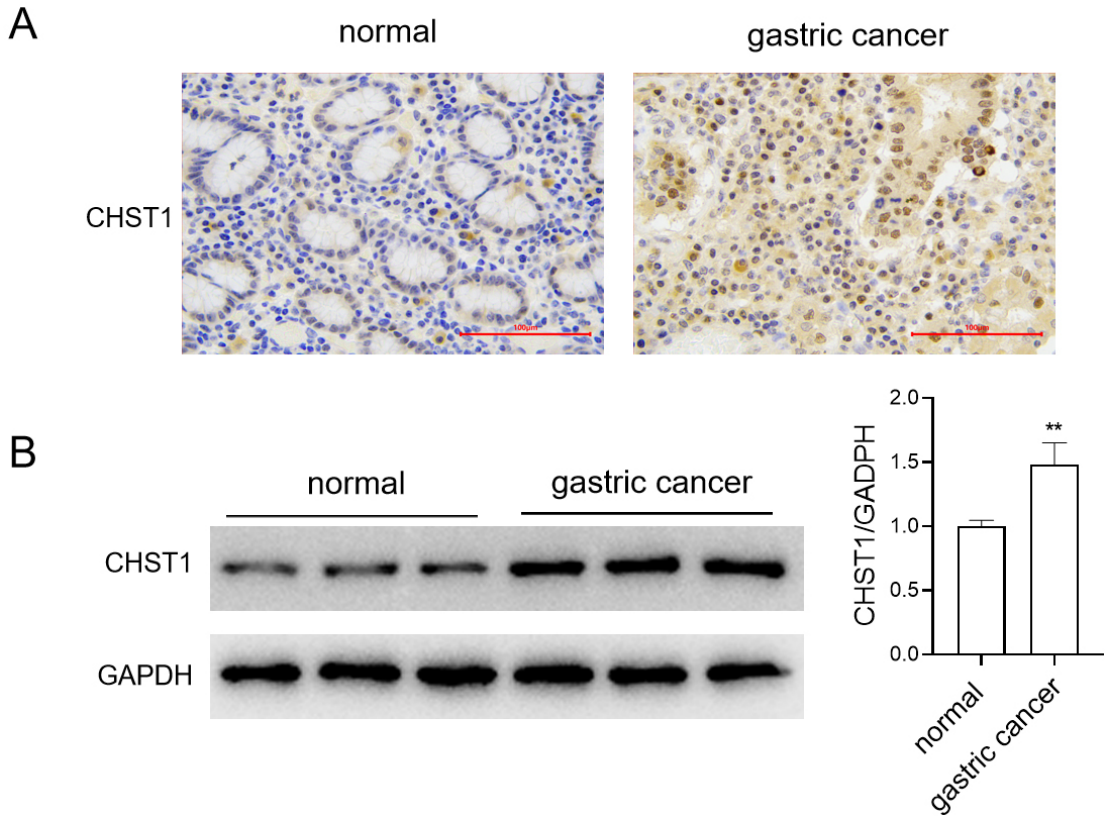

Fig. 9. Validation of CHST1 expression. (A) IHC validation of CHST1 expression in GC tissues. Scale bar = 100 µm. (B) WB analysis of CHST1 expression in GC tissues. Values are reported as mean ± SD (n = 3 independent replicates). ** $p < 0.01$ *vs*. normal. Between-group statistical comparisons were carried out using Student's *t*-test. IHC, immunohistochemistry; WB, western blot; SD, standard deviation.

($p < 0.05$, Fig. 8A). Survival analysis demonstrated that patients with high CHST1 expression exhibited poorer overall survival and shorter survival versus those with low CHST1 expression ($p < 0.05$, Fig. 8B). These findings suggest that high CHST1 expression is significantly related to the malignant progression and the unfavorable prognosis in GC.

3.8 Validation of CHST1 Expression in Clinical GC Tissues

CHST1 expression in patient-derived GC tissues was validated through IHC (Fig. 9A) and Western blot analysis (Fig. 9B). It was revealed that CHST1 protein expression was markedly increased in GC tissues versus normal tissues ($p < 0.01$).

3.9 Detection of CHST1 Expression in GC Cells

We found high CHST1 expression in GC cell lines (MKN28, HGC27, and AGS) relative to the gastric epithelial cell line GES-1 ($p < 0.05$), with the highest expression observed in AGS cells (Fig. 10A,B). Consistent results were obtained by IF analysis (Fig. 10C).

3.10 CHST1's Effect on Proliferation, Apoptosis, and Migration of AGS and HGC27 Cells

Given the highest CHST1 expression observed in AGS and HGC27 cells, these two cell lines were selected for carrying out subsequent experiments. Our findings showed that CHST1 protein expression was markedly lower in AGS and HGC27 cells in the sh-CHST1 group relative to the shRNA group ($p < 0.05$) (Fig. 11A,B). Consistently, low expression of CHST1 was found to markedly reduce proliferation of both AGS and HGC27 cells ($p < 0.05$) (Fig. 11C,D) but elevated the apoptosis rate (Fig. 11E). Additionally, decreased CHST1 expression led to a reduction in cell migration (Fig. 11F). These results suggest that inhibition of CHST1 suppresses GC cell proliferation and migration while enhancing apoptosis.

3.11 CHST1's Effect on the EMT of AGS and HGC27 Cells

Enhanced expression of the EMT-related protein E-cadherin and attenuated expression of N-cadherin, vimentin, and snail were found in the sh-CHST1 group relative to the shRNA group ($p < 0.05$) (Fig. 12A). Consistent results were observed by IF (Fig. 12B). It is suggested that CHST1 may be closely related to the EMT of AGS and HGC27 cells.

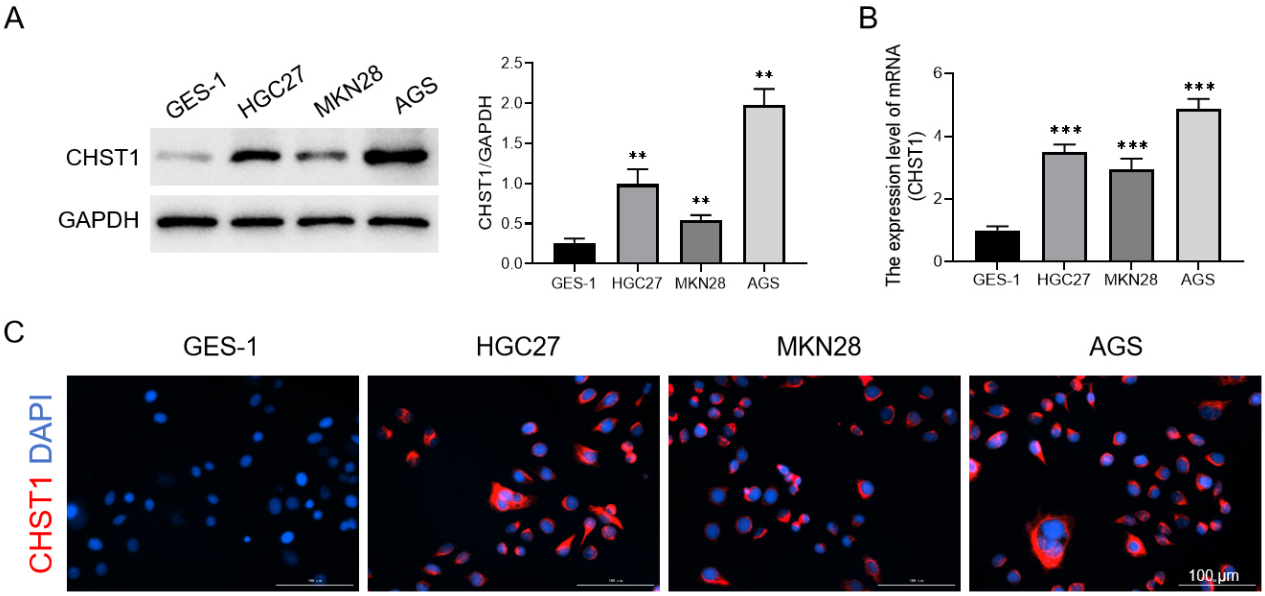

Fig. 10. Analysis of CHST1 expression in GC cell lines. (A) WB detection of CHST1 expression. (B) qRT-PCR detection of CHST1 expression. Values are reported as mean ± SD (n = 3 independent replicates). ** $p < 0.01$, *** $p < 0.001$ *vs*. GES-1. One-way ANOVA combined with Sidak's post hoc test. (C) IF detection of CHST1 expression. CHST1 is indicated by the red fluorescence signal, while cell nuclei were counterstained with DAPI (blue). Scale bar = 100 μm. CHST1, carbohydrate sulfotransferase 1; IF, immunofluorescence.

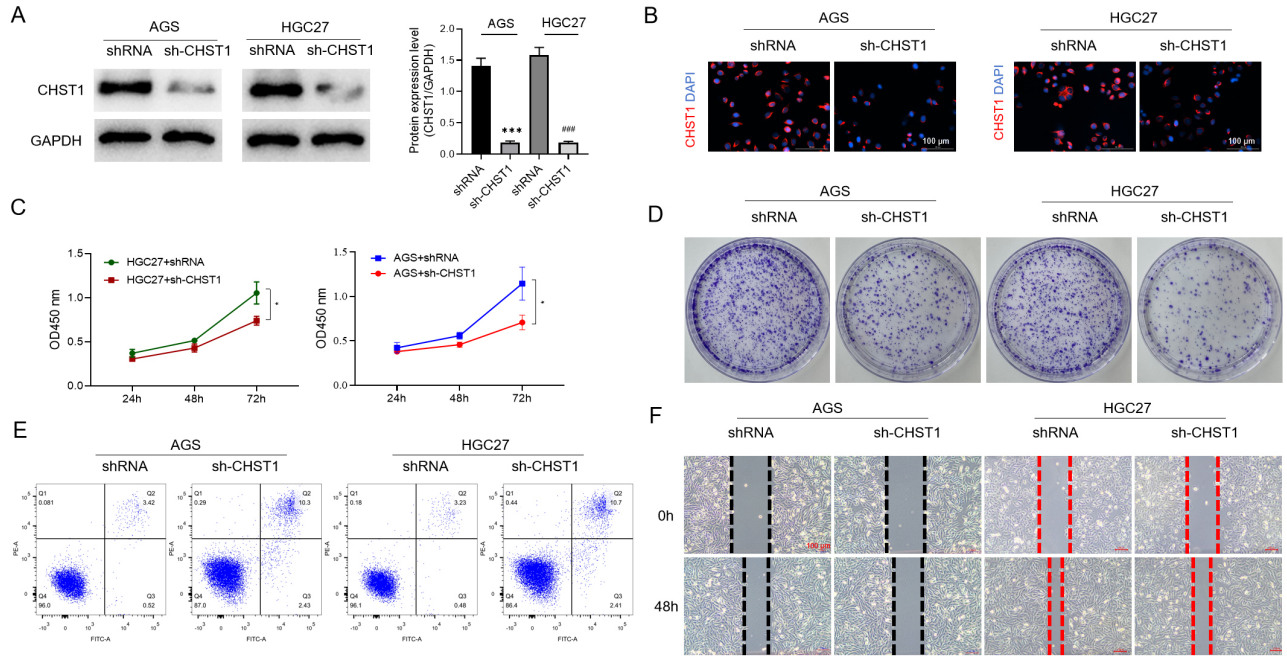

Fig. 11. Effects of CHST1 on the biofunctionality of AGS and HGC27 cells. (A) WB analysis to determine CHST1 expression. Values are reported as the mean ± SD (n = 3 independent replicates). *** $p < 0.001$ *vs*. AGS+shRNA group, ### $p < 0.001$ *vs*. HGC27+shRNA group. Between-group statistical comparisons were carried out using Student's *t*-test. (B) IF to detect CHST1 expression. CHST1 is indicated by the red fluorescence signal, while cell nuclei were counterstained with DAPI (blue). Scale bar = 100 μm. (C) CCK-8 assay to determine the proliferation of AGS and HGC27 cells. Values are reported as mean ± SD (n = 3 independent replicates). * $p < 0.05$. Between-group statistical comparisons were carried out using Student's *t*-test. (D) Plate cloning assay to detect cell proliferation. (E) Flow cytometry to determine cell apoptosis. (F) Scratch assay to determine cell migration. Scale bar = 100 μm. CHST1, carbohydrate sulfotransferase 1; sh-CHST1, CHST1 shRNA; CCK-8, Cell Counting Kit-8.

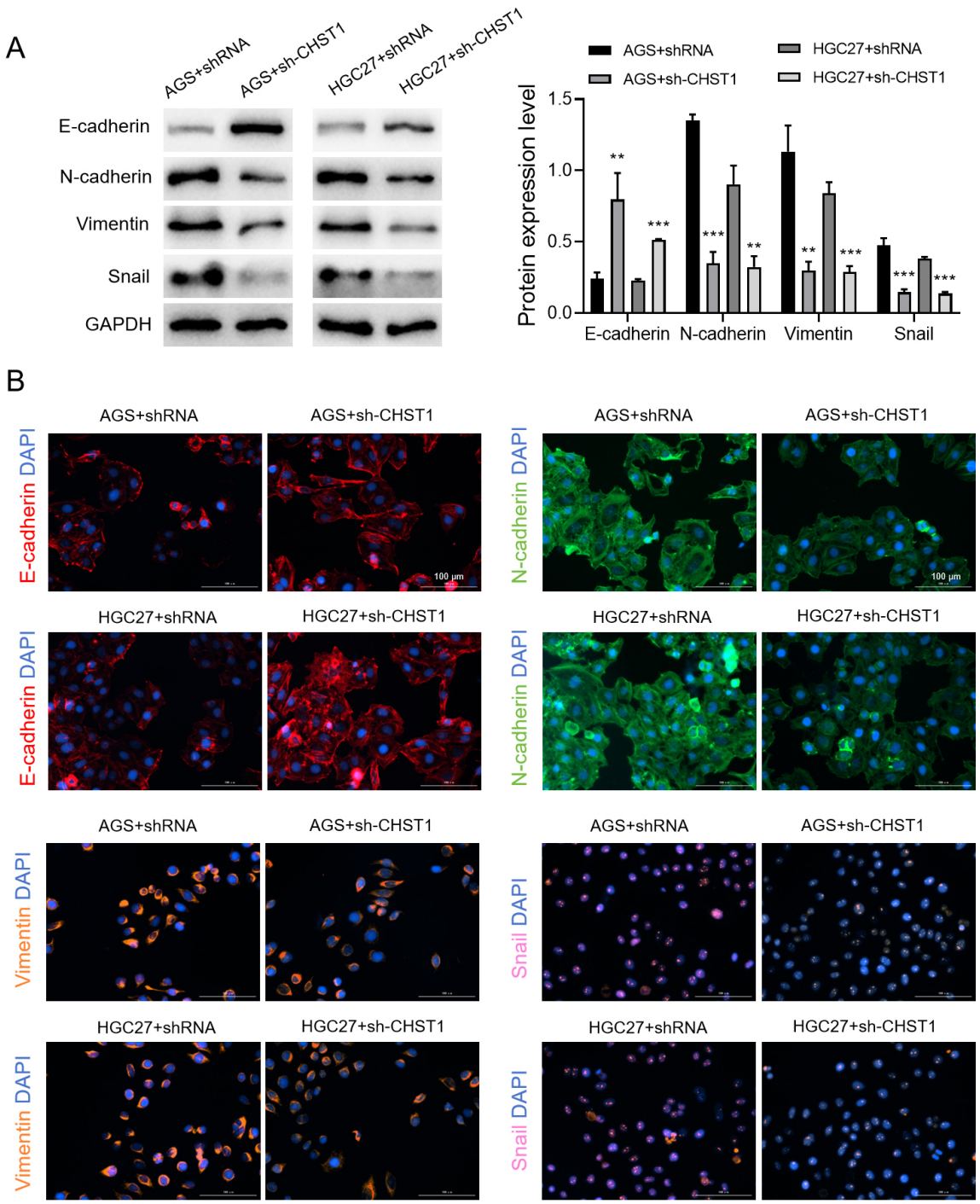

Fig. 12. Effects of CHST1 on the EMT of AGS and HGC27 cells. (A) WB analysis to determine the expression levels of EMT-related proteins. Values are reported as mean ± SD (n = 3 independent replicates). ** $p < 0.01$, *** $p < 0.001$. Between-group statistical comparisons were carried out using Student's *t*-test. (B) Detection of EMT-related proteins using IF. Cell nuclei were counterstained with DAPI (blue). Scale bar = 100 μm. CHST1, carbohydrate sulfotransferase 1; sh-CHST1, CHST1 shRNA.

3.12 CHST1 Modulates EMT and Malignant Phenotypes in AGS Cells via Regulation of the MAPK/ERK Signaling Pathway

Low expression of CHST1 suppressed the phosphorylation of p38 MAPK and ERK proteins in AGS cells ($p < 0.001$, Fig. 13A), whereas overexpression of CHST1 promoted the phosphorylation of these proteins ($p < 0.001$). Relative to the Control group, the SB203580 group exhibited significantly reduced cell proliferation ($p < 0.001$), decreased colony formation, increased apoptosis rate, and lower cell migration (Fig. 13B–E). Compared with the SB203580 group, the SB203580+OE-CHST1

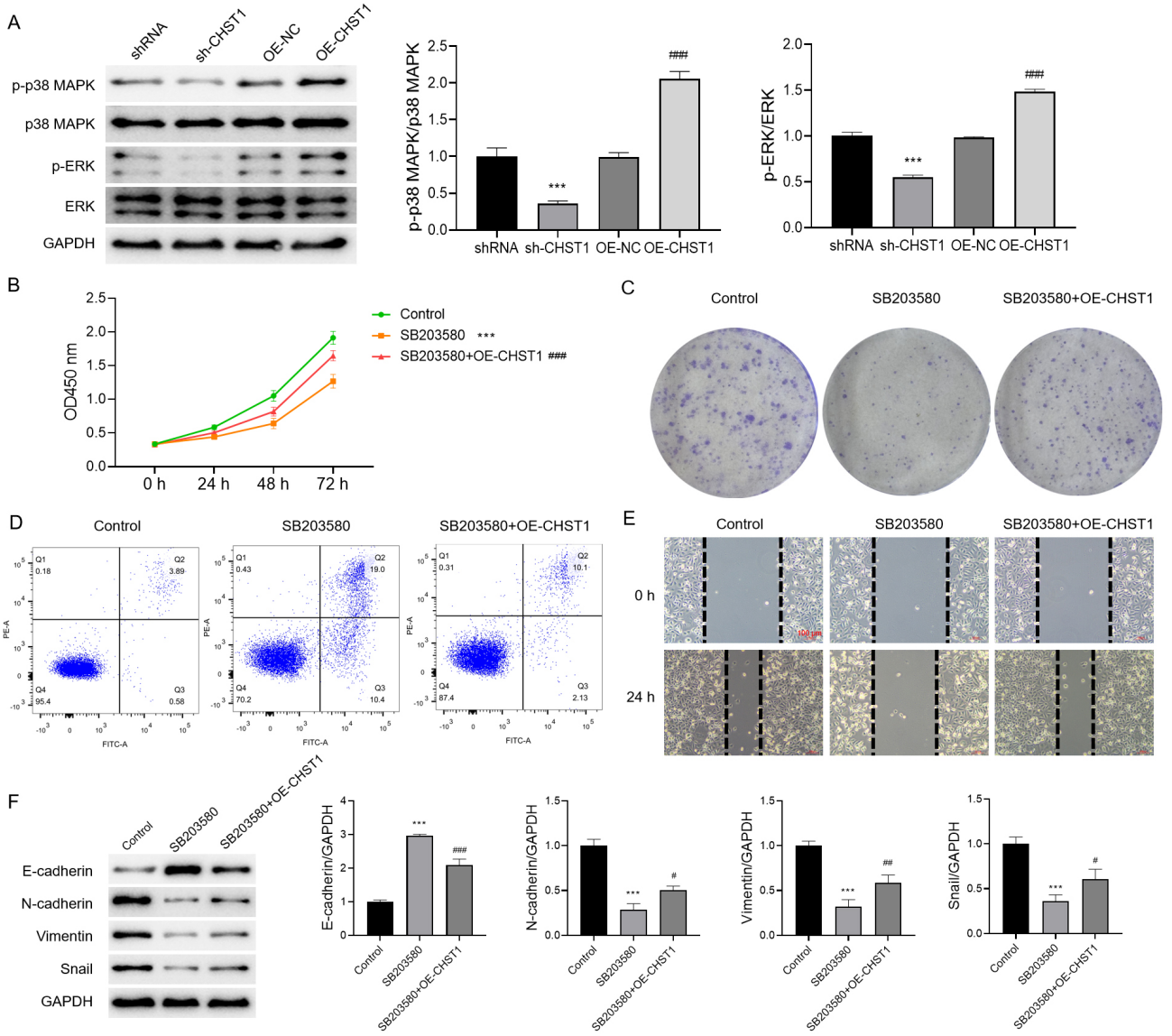

Fig. 13. CHST1 modulates EMT and malignant phenotypes in AGS cells via regulation of the MAPK/ERK signaling pathway. (A) WB analysis of CHST1's effect on the MAPK/ERK signaling pathway. Values are reported as mean ± SD (n = 3 independent replicates). Between-group statistical comparisons were carried out using Student's *t*-test. (B,C) Cell proliferation evaluated using CCK-8 and plate colony formation assays. (D) Apoptosis rate measured by flow cytometry. (E) Cell migration evaluated using the scratch assay. Scale bar = 100 µm. (F) WB analysis of EMT-related protein expression. Values are reported as mean ± SD (n = 3 independent replicates). *** $p < 0.001$ *vs.* shRNA or Control group; $^{\#}$ $p < 0.05$, $^{\#\#}$ $p < 0.01$, $^{\#\#\#}$ $p < 0.001$ *vs.* OE-NC or SB203580 group. One-way ANOVA combined with Sidak's post hoc test. CHST1, carbohydrate sulfotransferase 1; sh-CHST1, CHST1 shRNA; OE, CHST1 overexpression plasmid; OE-NC, overexpression empty plasmid; MAPK, mitogen-activated protein kinase; ERK, extracellular signal-regulated kinase.

group demonstrated markedly enhanced proliferation ($p < 0.001$), increased colony formation, decreased apoptosis rate, and improved cell migration. By contrast with the Control group, the SB203580 group had elevated E-cadherin protein expression ($p < 0.001$), but decreased expression of N-cadherin, vimentin, and snail proteins (Fig. 13F, $p < 0.001$). Relative to the SB203580 group, the SB203580+OE-CHST1 group showed decreased E-cadherin protein expression ($p < 0.001$), but elevated expression of N-cadherin, vimentin, and snail proteins ($p < 0.05$). Based on these results, it was indicated that CHST1 may promote EMT and malignant phenotypes in GC cells through the MAPK/ERK signaling pathway.

3.13 CHST1's Effect on AGS Cell Tumor Formation In Vivo

Subcutaneous tumor formation experiments in nude mice showed (Fig. 14A) that both the tumor volume and weight were higher in the AGS+shRNA group relative to

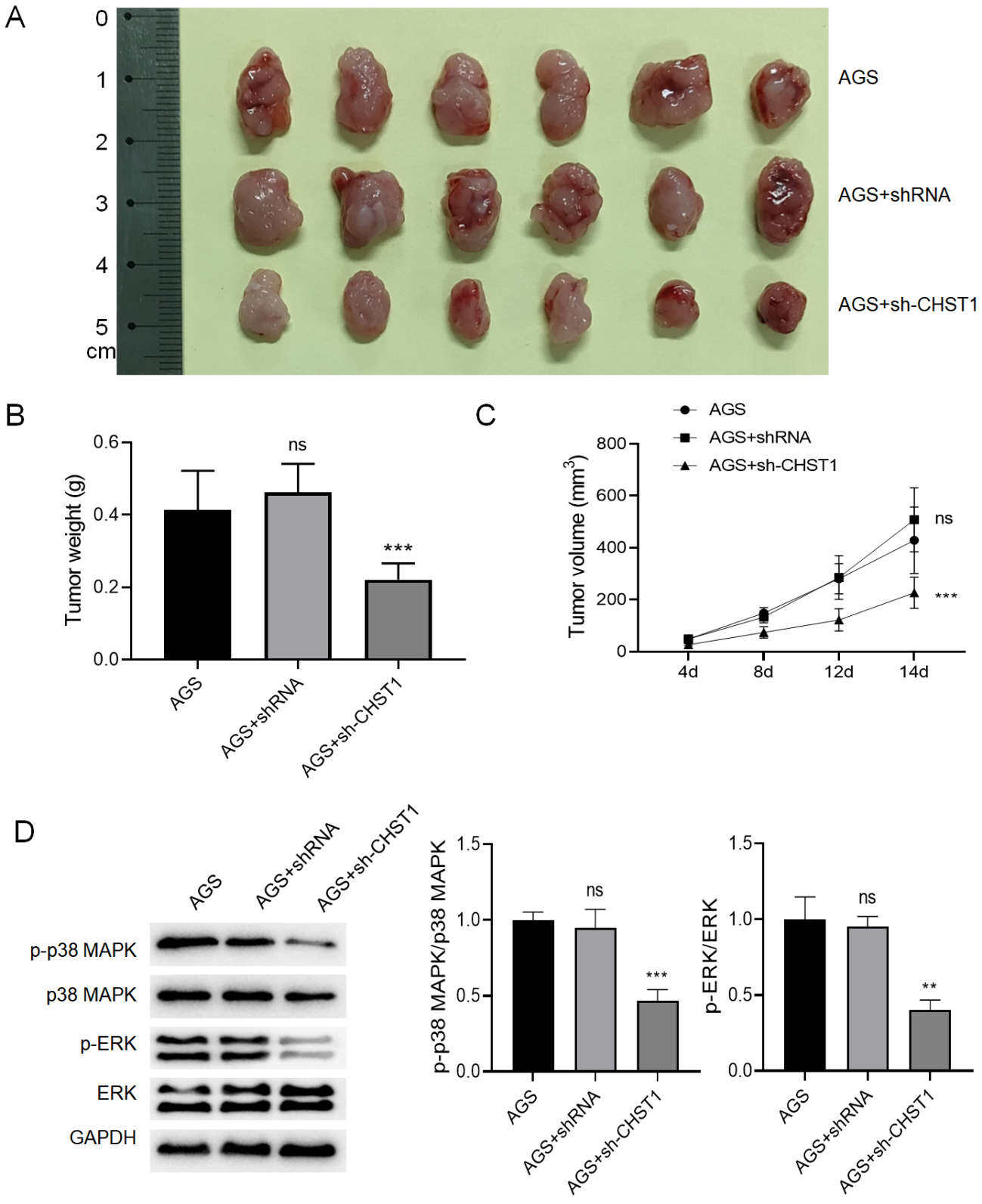

Fig. 14. Subcutaneous tumor formation in nude mice. (A) Morphology of subcutaneous tumor formation. (B) Comparison of the weight of subcutaneous tumor formation. Values are reported as mean ± SD (n = 6, six mice). (C) Comparison of the volume of subcutaneous tumor formation. Values are reported as mean ± SD (n = 6, six mice). (D) WB analysis of CHST1's effect on the MAPK/ERK signaling pathway. Values are reported as mean ± SD (n = 3 independent replicates). ns: $p > 0.05$ *vs*. AGS group, ** $p < 0.01$, *** $p < 0.001$ *vs*. AGS+shRNA group. One-way ANOVA combined with Sidak's post hoc test. CHST1, carbohydrate sulfotransferase 1; sh-CHST1, CHST1 shRNA.

the AGS+sh-CHST1 group ($p < 0.001$, Fig. 14B,C). In contrast, no marked difference was observed in tumor volume or weight between the AGS and the AGS+shRNA groups ($p > 0.05$). WB analysis revealed a significant decrease in the phosphorylation levels of p38 MAPK and ERK proteins in the AGS+sh-CHST1 group relative to the AGS+shRNA control group ($p < 0.01$, Fig. 14D). In contrast, no statistically significant difference was observed between the AGS parental and AGS+shRNA control groups ($p > 0.05$). These results suggest that CHST1 can significantly promote the growth of GC and enhance the activity of the MAPK/ERK signaling pathway.

4. Discussion

In recent years, early detection and treatment of GC have progressed rapidly in China, owing to the standardization and promotion of this cancer [16]. However, effective therapeutic options remain limited for individuals with advanced GC who have missed the opportunity for radical surgical resection [17]. Therefore, developing novel therapies for GC remains crucial.

In this study, publicly available transcriptomic data associated with GC were retrieved from TCGA. Bioinformatics analyses revealed a total of 4765 DEGs in GC tissues relative to normal tissues. Subsequent enrichment analysis illustrated that the predominant enrichment of these DEGs were linked to the ECM, which is closely related to EMT. It has been found that remodeling of the ECM can trigger EMT, as various EMT-inducing factors up-regulate the expression levels of proteases (e.g., matrix metalloproteinases) and some other ECM remodeling enzymes [18–20]. EMT represents an essential biological process through which malignant tumor cells derived from epithelial tissues, including those in GC, acquire migratory and invasive capabilities [21].

Therefore, we further investigated the correlation between GC tissues and EMT scores, revealing that the EMT score of GC tissues was highly significant in comparison to the normal tissues, suggesting a potential close association between GC and EMT. Subsequent WGCNA identified EMT-related modules and 50 key module genes. Functional enrichment analysis showed predominant enrichment of these key module genes in ECM, collagen, and protein uptake, which was consistent with the previous results. Finally, survival analysis identified seven significant survival-related genes, defined as hub genes (*CHST1*, *GPR176*, *OLFML2B*, *P4HA3*, *PDGFRB*, *SPARC*, and *VCAN*). Among these, CHST1 has been reported in several studies to be expressed at high levels in GC tissues [22–24]; however, the exact mechanism remains unclear.

In the subsequent analyses of this study, our findings illustrated that CHST1 was not only significantly and positively correlated with EMT, but also closely linked with the T-stage of GC. In summary, we hypothesized that CHST1 might modulate the EMT in GC tissues, thereby contributing to poor GC prognosis. To test the hypothesis, a series of cellular experiments was performed, which revealed high levels of CHST1 expression across GC cell lines. Knockdown of CHST1 suppressed the proliferation, colony formation, as well as migration of both AGS and HGC27 cells, while simultaneously promoting apoptosis. Additionally, inhibiting CHST1 led to up-regulation of E-cadherin (the epithelial-derived marker) and down-regulation of N-cadherin, vimentin, and snail (the mesenchymal-derived markers), indicating suppression of EMT and suggesting a close involvement of CHST1 in this process. The recent study has also reported that CHST1 promotes GC cell proliferation and metastasis [25], which aligns well with our experimental observations. Hence, it may be deduced that CHST1 holds potential as a novel therapeutic target in GC.

Recent investigations highlight the MAPK pathway as an important element in GC and a potential target for GC treatment [26–28]. Moreover, the MAPK pathway is also involved in regulating EMT across different types of cancers [29–31]. It can induce EMT by activating multiple transcription factors, thereby enhancing GC cell invasion and metastasis [32]. Our *in vitro* experiments revealed that CHST1 promotes MAPK/ERK pathway activity. More importantly, overexpression of CHST1 partially reversed SB203580's inhibitory effects on the proliferation, invasion, migration, and EMT of AGS cells, while also suppressing apoptosis triggered by SB203580. Our findings imply that CHST1 potentially promotes malignant behaviors, particularly EMT, by activating the MAPK/ERK pathway in GC cells. However, a limitation of this study is that the proposed mechanism has not yet been validated *in vivo*.

While this study establishes a key role for CHST1 in regulating the MAPK/ERK signaling pathway, a critical unresolved question is whether this function depends on its canonical glycosaminoglycan sulfotransferase activity. According to the enzyme activity-dependent hypothesis, CHST1 may influence receptor tyrosine kinase signaling indirectly by sulfating extracellular matrix or membrane-associated proteoglycans, thereby modulating ligand-receptor interactions or receptor clustering. Alternatively, the non-catalytic scaffolding hypothesis proposes that the CHST1 protein itself could act as an adaptor molecule, participating directly in the assembly of intracellular signaling complexes independent of its enzymatic function. Future investigations, such as functional comparisons between wild-type CHST1 and catalytically inactive point mutants, will be essential to delineate the underlying mechanism. Resolving this distinction is crucial for the rational development of CHST1-targeted therapeutic strategies aimed at precisely modulating relevant diseases, including cancer and fibrosis.

5. Conclusion

Through a detailed analysis of both GC and normal tissue samples obtained from TCGA using bioinformatics ap-

proaches, we successfully identified CHST1 as a key EMT-related gene linked with poor prognosis of GC. Through subsequent cellular experiments, CHST1 was confirmed to regulate EMT and malignant phenotypes via modulation of the MAPK/ERK pathway. The findings of this study provide a potential target for GC treatment. Nevertheless, the current study carries specific limitations that should be acknowledged. Further clinical and basic studies are required to confirm our finding that CHST1 enhances the poor prognosis of GC by modulating EMT. Our research team plans to explore this mechanism more deeply in subsequent studies.

Abbreviations

GC, Gastric cancer; CHST1, carbohydrate sulfotransferase 1; MAPK, mitogen-activated protein kinase; ERK, extracellular signal-regulated kinase; RNA-seq, RNA sequencing; TCGA, The Cancer Genome Atlas; WGCNA, weighted gene co-expression network analysis; EMT, Epithelial-mesenchymal transition; DEGs, Differentially Expressed Genes; GO, Gene Ontology; KEGG, Kyoto Encyclopedia of Genes and Genomes; CCK-8, Cell Counting Kit-8; sh-CHST1, CHST1 shRNA; GS, Gene Significance; MM, Module Membership.

Availability of Data and Materials

The datasets used and analysed during the current study are available from the corresponding author on reasonable request.

Author Contributions

XQ and YH: Conceptualization, Methodology, Formal Analysis, Validation, Writing—original draft; ZW: Data curation, Formal Analysis, Validation, Writing—review & editing; XZ: Investigation, Data curation, Visualization, Writing—review & editing; LS: Methodology, Supervision, Resources, Project administration, Writing—review & editing. All authors contributed to editorial changes in the manuscript. All authors read and approved the final manuscript. All authors have participated sufficiently in the work and agreed to be accountable for all aspects of the work.

Ethics Approval and Consent to Participate

All animal experiments were approved by the Experimental Animal Welfare Ethics Committee of the First Affiliated Hospital of Harbin Medical University (IACUC No. 2023068). All efforts were made to minimize suffering and reduce the number of animals used in accordance with the 3R principle. The use of human tissue samples was reviewed and approved by the Ethics Committee of the First Affiliated Hospital of Harbin Medical University (Approval No. 2024314). The gastric cancer tissue samples were provided by the Department of Gastroenterology, The First Affiliated Hospital of Harbin Medical University. Informed consent was obtained. The study was carried out in accordance with the guidelines of the Declaration of Helsinki.

Acknowledgment

Not applicable.

Funding

This work was supported by the Scientific Research Innovation Fund of The First Affiliated Hospital of Harbin Medical University (Grant number 2024M35).

Conflict of Interest

The authors declare no conflict of interest.

References

[1] Sung H, Ferlay J, Siegel RL, Laversanne M, Soerjomataram I, Jemal A, *et al*. Global Cancer Statistics 2020: GLOBOCAN Estimates of Incidence and Mortality Worldwide for 36 Cancers in 185 Countries. CA: a Cancer Journal for Clinicians. 2021; 71: 209–249. https://doi.org/10.3322/caac.21660.

[2] López MJ, Carbajal J, Alfaro AL, Saravia LG, Zanabria D, Araujo JM, *et al*. Characteristics of gastric cancer around the world. Critical Reviews in Oncology/hematology. 2023; 181: 103841. https://doi.org/10.1016/j.critrevonc.2022.103841.

[3] Zhou J, Dai Y, Zuo Z, Liu T, Li S. Famine Exposure during Early Life and Risk of Cancer in Adulthood: A Systematic Review and Meta-Analysis. The Journal of Nutrition, Health & Aging. 2023; 27: 550–558. https://doi.org/10.1007/s12603-023-1947-4.

[4] Huang Z, Hu Z, Wong LP, Lin Y. Determinants of gastric cancer screening attendance in Southeastern China: a cross-sectional study. BMJ Open. 2023; 13: e073925. https://doi.org/10.1136/bmjopen-2023-073925.

[5] Suzuki H, Oda I, Abe S, Sekiguchi M, Mori G, Nonaka S, *et al*. High rate of 5-year survival among patients with early gastric cancer undergoing curative endoscopic submucosal dissection. Gastric Cancer. 2016; 19: 198–205. https://doi.org/10.1007/s10120-015-0469-0.

[6] Long VD, Dat TQ, Thong DQ, Hai NV, Le Minh Quoc H, Nguyen DT, *et al*. Long-Term Outcomes of Open Versus Laparoscopic Distal Gastrectomy for T4a Gastric Cancer: A Propensity Score-Matched Cohort Study. Annals of Surgical Oncology. 2023; 30: 2278–2289. https://doi.org/10.1245/s10434-022-12897-z.

[7] Castaneda M, den Hollander P, Kuburich NA, Rosen JM, Mani SA. Mechanisms of cancer metastasis. Seminars in Cancer Biology. 2022; 87: 17–31. https://doi.org/10.1016/j.semcancer.2022.10.006.

[8] Huang Y, Hong W, Wei X. The molecular mechanisms and therapeutic strategies of EMT in tumor progression and metastasis. Journal of Hematology & Oncology. 2022; 15: 129. https://doi.org/10.1186/s13045-022-01347-8.

[9] Zhan J, Zhou L, Zhang H, Zhou J, He Y, Hu T, *et al*. A comprehensive analysis of the expression, immune infiltration, prognosis and partial experimental validation of CHST family genes in gastric cancer. Translational Oncology. 2024; 40: 101843. https://doi.org/10.1016/j.tranon.2023.101843.

[10] Wang D, Liu B, Zhang Z. Accelerating the understanding of cancer biology through the lens of genomics. Cell. 2023; 186: 1755–1771. https://doi.org/10.1016/j.cell.2023.02.015.

[11] Huang S, Zhang Y, Shu H, Liu W, Zhou X, Zhou X. Advances of the MAPK pathway in the treatment of spinal cord injury.

CNS Neuroscience & Therapeutics. 2024; 30: e14807. https://doi.org/10.1111/cns.14807.

[12] Ye J, Wang J, Liu R, Chen C, Wang W. The prognostic significance and potential mechanism of PFDN4 in hepatocellular carcinoma. International Immunopharmacology. 2025; 145: 113761. https://doi.org/10.1016/j.intimp.2024.113761.

[13] Yuan J, Dong X, Yap J, Hu J. The MAPK and AMPK signalings: interplay and implication in targeted cancer therapy. Journal of Hematology & Oncology. 2020; 13: 113. https://doi.org/10.1186/s13045-020-00949-4.

[14] Cho W, Jin X, Pang J, Wang Y, Mivechi NF, Moskophidis D. The Molecular Chaperone Heat Shock Protein 70 Controls Liver Cancer Initiation and Progression by Regulating Adaptive DNA Damage and Mitogen-Activated Protein Kinase/Extracellular Signal-Regulated Kinase Signaling Pathways. Molecular and Cellular Biology. 2019; 39: e00391-18. https://doi.org/10.1128/MCB.00391-18.

[15] Yuan W, Shi Y, Dai S, Deng M, Zhu K, Xu Y, *et al*. The role of MAPK pathway in gastric cancer: unveiling molecular crosstalk and therapeutic prospects. Journal of Translational Medicine. 2024; 22: 1142. https://doi.org/10.1186/s12967-024-05998-8.

[16] Guo X, Peng Y, Song Q, Wei J, Wang X, Ru Y, *et al*. A Liquid Biopsy Signature for the Early Detection of Gastric Cancer in Patients. Gastroenterology. 2023; 165: 402–413.e13. https://doi.org/10.1053/j.gastro.2023.02.044.

[17] Guan WL, He Y, Xu RH. Gastric cancer treatment: recent progress and future perspectives. Journal of Hematology & Oncology. 2023; 16: 57. https://doi.org/10.1186/s13045-023-01451-3.

[18] Peng D, Fu M, Wang M, Wei Y, Wei X. Targeting TGF-β signal transduction for fibrosis and cancer therapy. Molecular Cancer. 2022; 21: 104. https://doi.org/10.1186/s12943-022-01569-x.

[19] Paolillo M, Schinelli S. Extracellular Matrix Alterations in Metastatic Processes. International Journal of Molecular Sciences. 2019; 20: 4947. https://doi.org/10.3390/ijms20194947.

[20] Peng L, Wen L, Shi QF, Gao F, Huang B, Meng J, *et al*. Scutellarin ameliorates pulmonary fibrosis through inhibiting NF-κB/NLRP3-mediated epithelial-mesenchymal transition and inflammation. Cell Death & Disease. 2020; 11: 978. https://doi.org/10.1038/s41419-020-03178-2.

[21] Zhang M, Cao C, Li X, Gu Q, Xu Y, Zhu Z, *et al*. Five EMT-related genes signature predicts overall survival and immune environment in microsatellite instability-high gastric cancer. Cancer Medicine. 2023; 12: 2075–2088. https://doi.org/10.1002/cam4.4975.

[22] Vafaeie F, Nomiri S, Ranjbaran J, Safarpour H. ACAN, MDFI, and CHST1 as Candidate Genes in Gastric Cancer: A Comprehensive Insilco Analysis. Asian Pacific Journal of Cancer Prevention. 2022; 23: 683–694. https://doi.org/10.31557/APJCP.2022.23.2.683.

[23] Li R, Jiang WJ, Jin SL, Zhao RH, Cao XG, Zong H. Construction and analysis of competitive endogenous RNA regulatory network related to gastric cancer. Zhonghua Zhong Liu Za Zhi. 2020; 42: 115–121. https://doi.org/10.3760/cma.j.issn.0253-3766.2020.02.006. (In Chinese)

[24] Yang Y, Chen Z, Zhou L, Wu G, Ma X, Zheng Y, *et al*. *In silico* development and validation of a novel glucose and lipid metabolism-related gene signature in gastric cancer. Translational Cancer Research. 2022; 11: 1977–1993. https://doi.org/10.21037/tcr-22-168.

[25] Gui L, Yu JH, Tan JN, Zhong GY, Wang YX, Zhong L, *et al*. CHST1 as a prognostic-related biomarker in gastric cancer correlating with immune infiltration. Heliyon. 2025; 11: e42124. https://doi.org/10.1016/j.heliyon.2025.e42124.

[26] Ma F, Yao J, Niu X, Zhang J, Shi D, Da M. MARK4 promotes the malignant phenotype of gastric cancer through the MAPK/ERK signaling pathway. Pathology, Research and Practice. 2024; 261: 155471. https://doi.org/10.1016/j.prp.2024.155471.

[27] Ma L, Hu X, Zhang W, Qi D, Chen L, Yin M. Weifuchun suppresses the malignancy of gastric cancer cells by targeting KPNA2 through miR-26a-5p-mediated destabilization and the deactivation of the MAPK signaling pathway. Journal of Ethnopharmacology. 2024; 334: 118538. https://doi.org/10.1016/j.jep.2024.118538.

[28] Miao X, Liu Y, Fan Y, Wang G, Zhu H. LncRNA BANCR Attenuates the Killing Capacity of Cisplatin on Gastric Cancer Cell Through the ERK1/2 Pathway. Cancer Management and Research. 2021; 13: 287–296. https://doi.org/10.2147/CMAR.S269679.

[29] Wang H, Liang S, Du X, Zhao G, Bai Y, Li J, *et al*. RAB26 promotes prostate cancer progression via the MAPK/ERK-TWIST1 signaling axis. Genes & Diseases. 2025; 12: 101689. https://doi.org/10.1016/j.gendis.2025.101689.

[30] Hu Q, Chen X. MiR-27a-3p Enhances Endometrial Cancer Growth and EMT by Targeting LIFR and Activating the p38/MAPK Pathways. Iranian Journal of Biotechnology. 2025; 23: e4008. https://doi.org/10.30498/ijb.2025.483853.4008.

[31] Song YJ, Kim JE, Rajbongshi L, Lim YS, Ok YJ, Hwang SY, *et al*. Silencing of Epidermal Growth Factor-like Domain 8 Promotes Proliferation and Cancer Aggressiveness in Human Ovarian Cancer Cells by Activating ERK/MAPK Signaling Cascades. International Journal of Molecular Sciences. 2024; 26: 274. https://doi.org/10.3390/ijms26010274.

[32] Sun B, Zhong FJ. ELTD1 Promotes Gastric Cancer Cell Proliferation, Invasion and Epithelial-Mesenchymal Transition Through MAPK/ERK Signaling by Regulating CSK. International Journal of General Medicine. 2021; 14: 4897–4911. https://doi.org/10.2147/IJGM.S325495.